

Static Failure Analysis of Composite Tube with Ply Drops Subjected to Combined Bending and Compression Loads

Inés Ruiz Pastor^a

^aDepartment of Mechanical and Manufacturing Engineering, Aalborg University, Fibigerstræde 16, Aalborg DK-9220, Denmark

Abstract

Fibre composite materials provide high stiffness and strength to weight ratio compared to typical engineering metals, which makes them a favoured material for light weight structural applications. However, when optimizing the material use in composite structures, thickness tailoring is often required but it consequently lead to ply drops. Ply drops lead to stress concentrations and specially in compression it may resolve in premature failure of the structure.

This paper investigates an alternative experimental test setup for studying compression failure of the composites with an embedded ply drop. This setup introduces a combined compression and bending loading to a unidirectional glass reinforced composite tube which contains ply drops. This combined loading state is achieved by applying eccentric compression force to the tube. Experimental observations confirm that failure initiation occurs in the ply drop and progress as delamination followed by kink-banding mechanism that led to fibre failure. A finite element model of the setup is used to analyse which possible stress component provokes failure initiation. Furthermore, the far field stress state of the composite tube is studied to examine the similarities/discrepancies from the typically used "flat type specimen". It was found that even the far field stresses are slightly more complex compared to the alternative "flat type specimen" and the tube setup could possibly be used as benchmark case for compression models of composite material with embedded ply drops.

Keywords: Unidirectional composite tube, Ply drop, Eccentric compression, Kink-banding, FEM

1. Introduction

Fibre reinforced composite structures are present in a large number of engineering applications. This material has become popular because it provides the structural design engineers with the ability to tailor the material properties to given structural requirements and thus studies in this field are increasing rapidly. In many composite structures ply terminations (ply drops) are introduced in the attempt to optimize the material use. These however act as weak points in the structure since stress concentrations are introduced due to material discontinuities. Among all engineering structures, tubular shapes are the most commonly used, however they tend to fail abruptly and catastrophically.

A considerable amount of investigations have been published focusing on the response of tubular composites to the different loads that are shown in Figure 1.

Jelf and Fleck [1] studied the compressive strength of unidirectional composite tubes under combined compression and torsion. They concluded that failure mechanism was plastic microbuckling, which is a plastic shear instability that occurs when the shear yield strength of the matrix is reached. Fibre misalignments ease this kind of failure. They also observed that axial compressive strength decreased in a linear manner with increasing applied shear stress. Later, Harte and Fleck [2]

repeated the study this time by the use of braided composite tubes. They mapped failure modes as a function of braid angle.

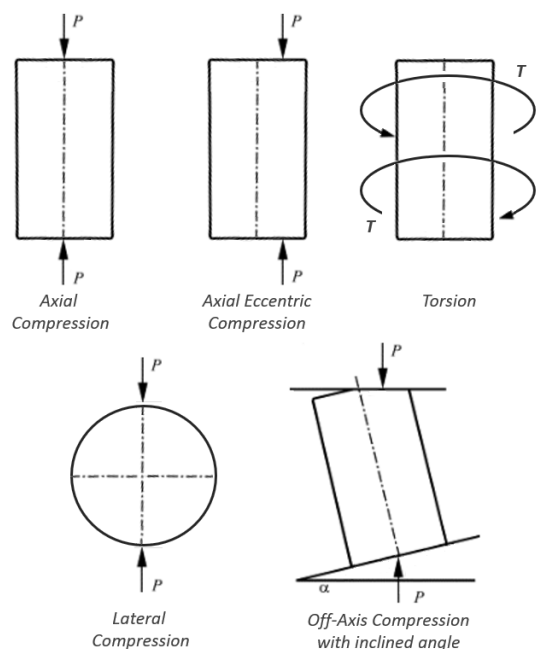


Figure 1: Loading cases that have been studied.

*Corresponding author E-mail address: iruiz16@student.aau.dk

Dominant failure mode for compression loading were fibre

microbuckling and diamond shaped buckling (triggered by the braiding of the fibres) and microbuckling in torsion. McGregor et al. [3] continued the damage development study in braided composite tubes under axial compression. Predicting response under axial compression is complicated due to the complex nature of failure mechanisms, however they succeeded in simulating damage initiation, growth and final failure. Abdewi [4] tested composite tubes with different corrugation profiles under lateral compression to prove the effect of corrugation on the crushing behaviour and failure mechanism.



Figure 2: Corrugated profiles tested by Abdewi [4].

He concluded that corrugation did not affect the lateral crushing behaviour as he obtained similar results compared to the flat cylinder. Then, Abdewi et al. [5] studied both axial and lateral crushing of the aforementioned radial corrugated composite tubes. They concluded that structure shape for axial crushing affects failure mode and energy absorption capability significantly, as they found that corrugated profiles absorbed 4 times more energy than flat round profile. However, it was again proved that no effect was observed for lateral crushing.

The fact that composite cylinders loaded under pure compression fail at stresses below the compressive strengths seem predominant in many investigations. Daniel et al. [6] investigated failure mechanisms in thick composites under compressive loading. They stated that early failures could have been caused by fibre misalignments/waviness (phenomenon also studied by Wang et al. [7]) and non linear behaviour of the matrix. They concluded that matrix shear yielding was the failure mechanism followed by fibre buckling in the form of kink band and fracture.

As seen, several studies have been performed on composite tubes under axial compression but one of the most common features has been kept out. In reality, many optimized composite structure involve dropping internal plies to achieve variation in thickness. Steeves and Fleck [8] investigated the failure of composite laminates with terminated internal plies under axial compression. However, they tested flat specimens concluding that failure mechanism was caused by microbuckling of the longitudinal fibres near the toe of the resin pocket, or by delamination near the heel of the resin pocket.

As well as the presence of resin pockets in real structures, components are commonly subjected not only to axial compression. Song and Du [9] investigated off-axis crushing of glass fibre reinforced composite tubes, introducing an inclination angle of loading with respect to the tube axis (see Figure 1). They concluded that energy absorption decreased as the off-axis in-

clination angle increased since specimens showed a strong tendency of collapsing at large off-axis angles.

Based on the literature review conducted it seems that composite tubes subjected to a combined compression and pure bending loads has not been examined to the same extent as compression-torsion loaded tubes. The compression-bending load combination is believed to provide a well defined and local stress intense area. In this paper this will be used to study failure near a ply-drop. This paper combines the study of failure mechanism and crack development of a composite tube containing ply drops with the application of non-concentric compression load, which will create the load combination "compression-bending". It is mainly focused on an experimental approach also supported by finite element analysis and it is organized as follows. First, the composite specimen is described in Section 2. Then the experimental test campaign as well as the finite element model are presented in Section 3 and 4, respectively. Finally, Section 5 contains a summary of the obtained results and conclusions.

2. Testing specimen

2.1. Material and geometry

Cylindrical composite tubes with internal ply drops were manufactured from E-Glass fibres (reinforcement) and polyester resin (matrix). This work has been developed in collaboration with a Ph.D research [10] from which properties of the composite (Table 1) were obtained from.

Parameter	Value
E_{11}	45.473 GPa
E_{22}, E_{33}	14.075 GPa
ν_{12}, ν_{13}	0.26
ν_{23}	0.5
G_{12}, G_{13}	4.884 GPa
G_{23}	2.50 GPa
$S_{11} (C)$	579 MPa
$S_{11} (T)$	870 MPa
$S_{22}, S_{33} (C)$	149 MPa
$S_{22}, S_{33} (T)$	36 MPa
S_{12}, S_{13}	55 MPa
S_{23}	47 MPa

Table 1: E-Glass/polyester unidirectional composite properties obtained from a Ph.D research collaboration [10], where 1 is fibre direction. $S_{ij} (C)$ refers to compressive strength and $S_{ij} (T)$ to tensile strength.

The lay-up consisted of six unidirectional plies where two were terminated forming a [6-2-4] ply drop (see Figure 3). All fibres are aligned with the longitudinal axis of the tube. Three specimens were manufactured whose total length were 150 mm. The inner diameter was 75 mm and ply thickness was measured to be 0.95 mm from the specimens.

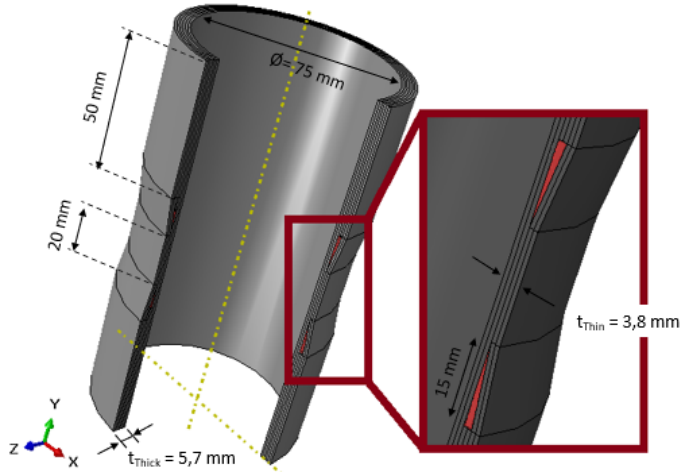


Figure 3: Specimen geometry. A 90° cut has been done to show lay-up. Red color represents resin pockets.

2.2. Fabrication process

The composite tubes were manufactured by rolling dry fibreglass material onto a mandrel of 75 mm circular diameter. Then, the component was introduced into a bag where vacuum was applied. Polyester resin was injected and left curing for 24 hours at room temperature. This manufacturing process is known as Vacuum Assisted Resin Transfer Moulding (VARTM) [11]. After the curing was completed, the mandrel was removed by the use of a hydraulic press and three tube specimens were cut.

3. Experimental Testing

Experimental test campaign consisted of applying a compression load in two different configurations: one aligned with the cylinder longitudinal axis and the other exhibiting eccentricity with respect to the central axis. When a load is applied to a circular annulus, accounting for possible eccentricity, some reaction is expected in the round surface following an unknown stress distribution function. This distribution can be obtained by applying force equilibrium and a moment equilibrium, leading to the following function (see Appendix A for the full development of the expression):

$$q(\theta) = \frac{F}{2\pi R t} + \frac{F a \cos \theta}{\pi R^2 t} \quad (1)$$

where $q(\theta)$ is the function that represents the stress along the circumference (θ is the angle measured counter-clockwise from the x axis, see Figure 4), F the force applied, R the middle radius of the annulus, t the thickness and a the eccentricity. Figure 4 shows this stress distribution function when 1 kN is applied as well as a MATLAB contour plot on a circular annulus to ease its comprehension. Eccentric compression force adds a bending moment on the component concentrating the stresses to a well defined area of the tube.

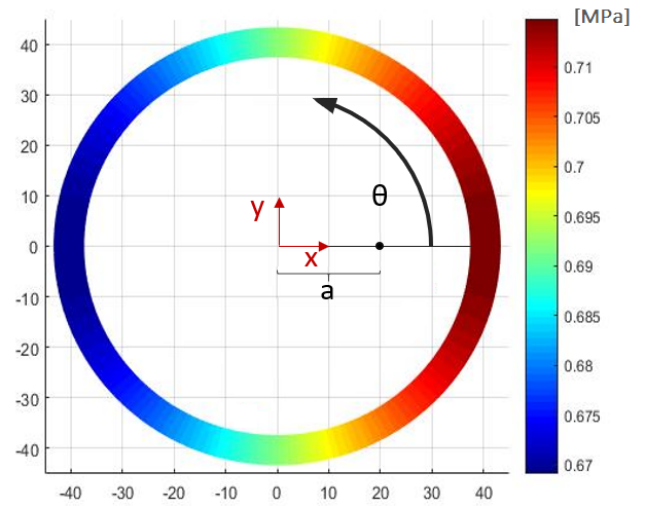
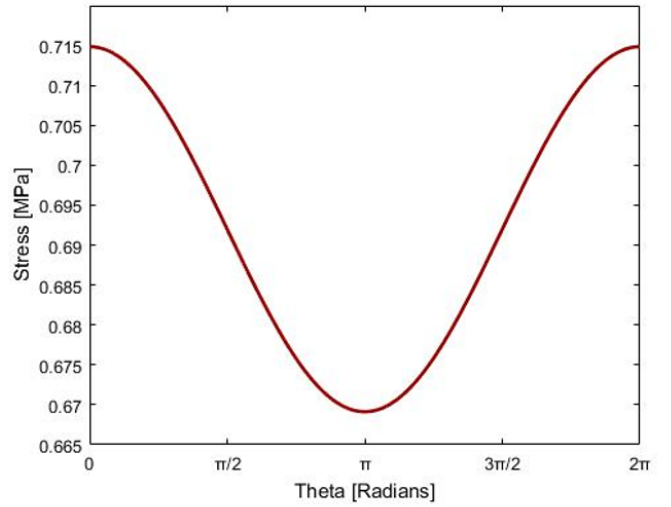


Figure 4: Stress distribution along a circular annulus for a compression force of 1 kN with eccentricity $a = 2R/3$ respect to the centre (black dot).

3.1. Setup and procedure

Test setup is sketched in Figure 5, however pictures from the physical experiment can be consulted at Appendix B. The tubular specimen is placed in between two steel round plates with multiple circular grooves allowing for the specimens of different diameter. On the back side, the plates have round marks at different distances from the centre to allow force application with different eccentricities a (Technical drawing of the plates is attached at Appendix C). The method to introduce the compression force to one specific location is through two steel balls.

The test machine used is a Schenk 400 kN hydraulic test machine with an Instron controller. The specimens were loaded quasi statically using displacement control. A first test was carried out applying the force on the centre of the tube. This led to a uniform stress distribution along the circumferential surface. Test displacement rate was set to be 0.5 mm/sec. Results from this test are compared to the finite element model to

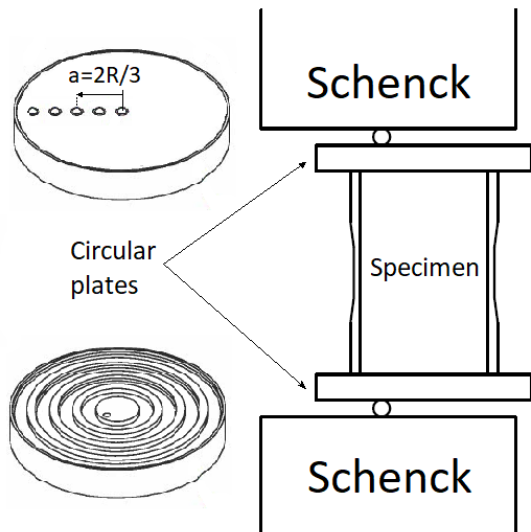


Figure 5: Setup cross section view sketch where load is applied with some eccentricity.

check reliability. Next, two tests were performed applying the force at $2/3$ of the radius measured from the centre of the cylinder. Now, stress distribution along the circumferential surface is not uniform thus the response of the component will be to compression and bending.

In one of the tests, displacement rate was kept 0.5 mm/sec and a digital camera was placed to record crack initiation. On the other test, displacement control was lowered down to 0.05 mm/sec and single strain gauges were glued to the specimen, longitudinally aligned, to get strain fields at different locations along the circumference (see Figure 6). Table 2 summarizes test conditions.

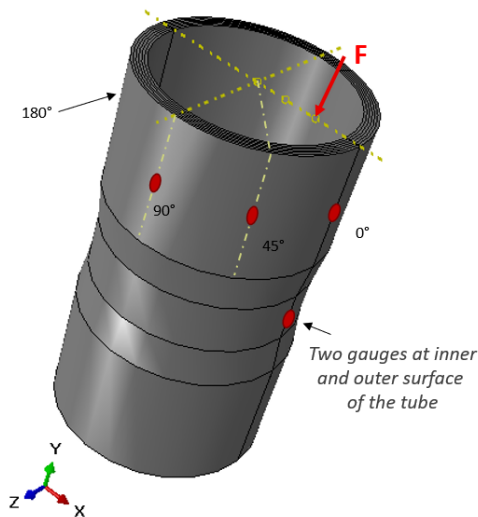


Figure 6: Strain Gauge placement in the composite specimen.

Test Num.	a	Displ. Rate [mm/sec]	Output
Test 1	0	0.5	Force vs. Displ
Test 2	$2R/3$	0.5	Failure recording
Test 3	$2R/3$	0.05	Force vs. Displ + Strain (from SG)

Table 2: Test conditions and output for each.

3.2. Test results

When the compression load was applied to the central axis of the tube, composite specimen withstood a compressive load of 188 kN. Failure was a sudden event that entailed fibre fracture along the whole circumference at the upper ply drop location. Load-Displacement data obtained is shown in Figure 7.

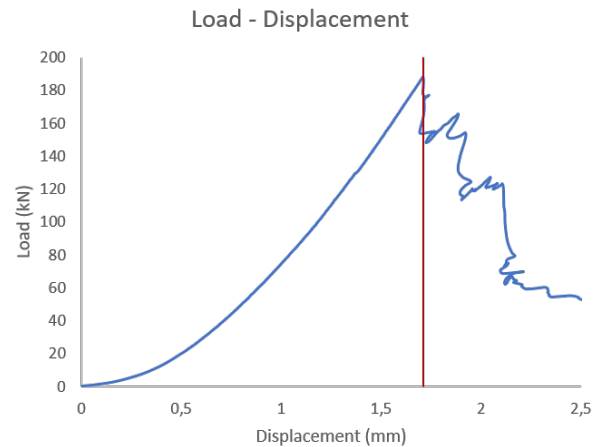


Figure 7: Load - Displacement curve when compression load is centred.

The maximum displacement that the composite tube could exhibit before failure was 1.71 mm, after which the event of failure seems to be a sequence of damage progress.

When the loading point was moved to $2/3$ of the radius measured from the centre, failure load decreased to 138 kN and 135 kN in these tests. A digital camera captured the initial delamination at 110 kN prior to the final failure at 138 kN:

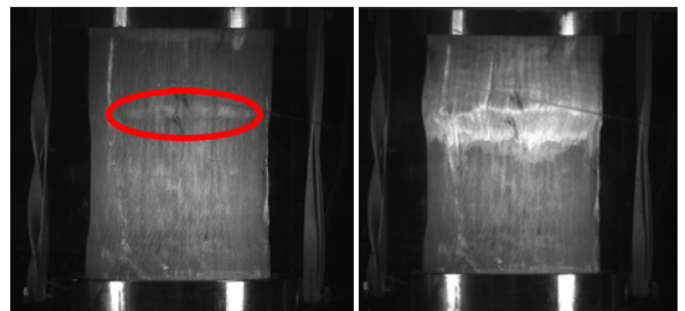


Figure 8: Left image captured delamination initiation. As it is a sudden event, next frame (right image) shows fibre fracture.

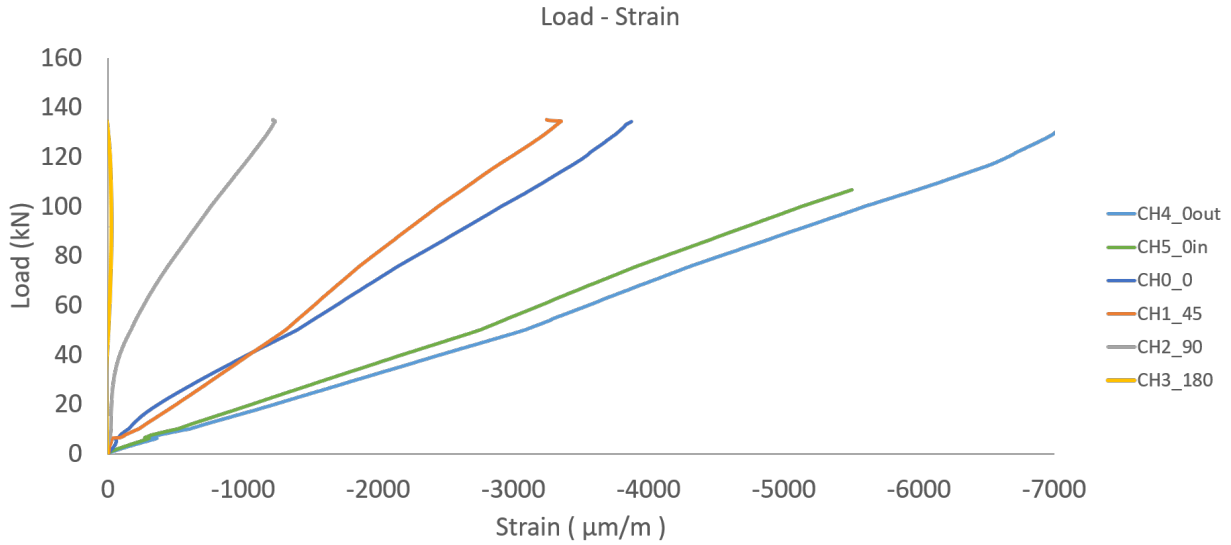


Figure 9: Strain gauge measurements from Test 3.

Strain gauge measurements on the second tube tested at this load configuration showed strain at different locations on the tube (see Figure 6 and Figure 9). Strain measured by both strain gauges at the thin part of the tube (*CH4_0out* and *CH5_0in*, in the graph) are significantly larger compared to strain data on the thick part as expected. The small difference between both readings show that a slight bending was present on the thin section. Then, strains at 0° and 45° become quite similar as both locations are close to the load application point.

Differences arise for 90° and even more for 180°, where strains are negligible compared to the rest of readings. This means that if the load is applied further away from the tube centre, the opposite extreme of the tube would not be loaded in compression. Figure 10 show the Load-Displacement from Test 3. Data from Test 2 was disregarded due to plastic deformation of the steel plates that affected the displacement measurements obtained.

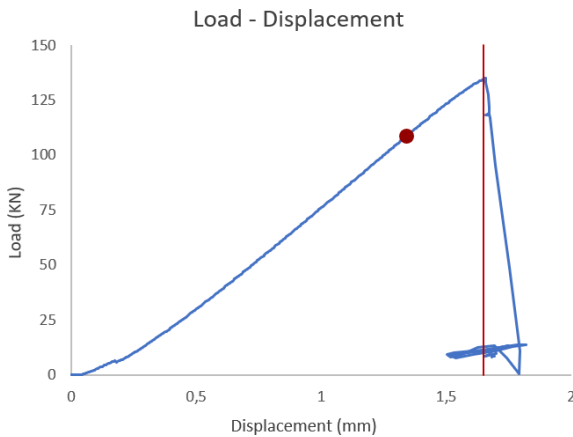


Figure 10: Load - Displacement curve when compression load is eccentric. Red dot represents initial delamination.

3.3. Discussion on the event of damage

It was not possible to get an insight of the crack development from the image recording. The crack front occupied half of the tube as shown in Figure 12 (which represents the tube seen from above). The real broken specimen can be seen in Appendix D), so it was decided to perform some cuts along the crack to see if it was possible to identify the crack development. Unfortunately, cuts from 0° to 60° looked similar, therefore no conclusion could have been obtained. This matches the strain gauge similar readings for both gauges located at 0° and 45° meaning that the expected damage should be equivalent. All these cuts are included in Appendix D. As crack started at 90°, several small cuts were performed at the vicinity of the crack (at the blue circle of the Figure 12) to capture the failure mechanism.

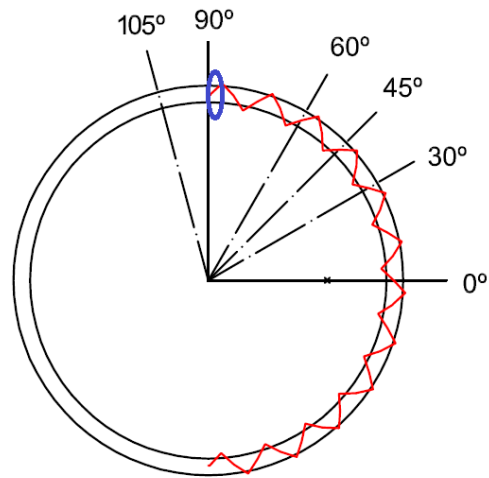


Figure 12: Longitudinal cuts made on the specimen along the crack, represented by the red zig-zag line. Cut at 105° was done to check if the section remained intact.

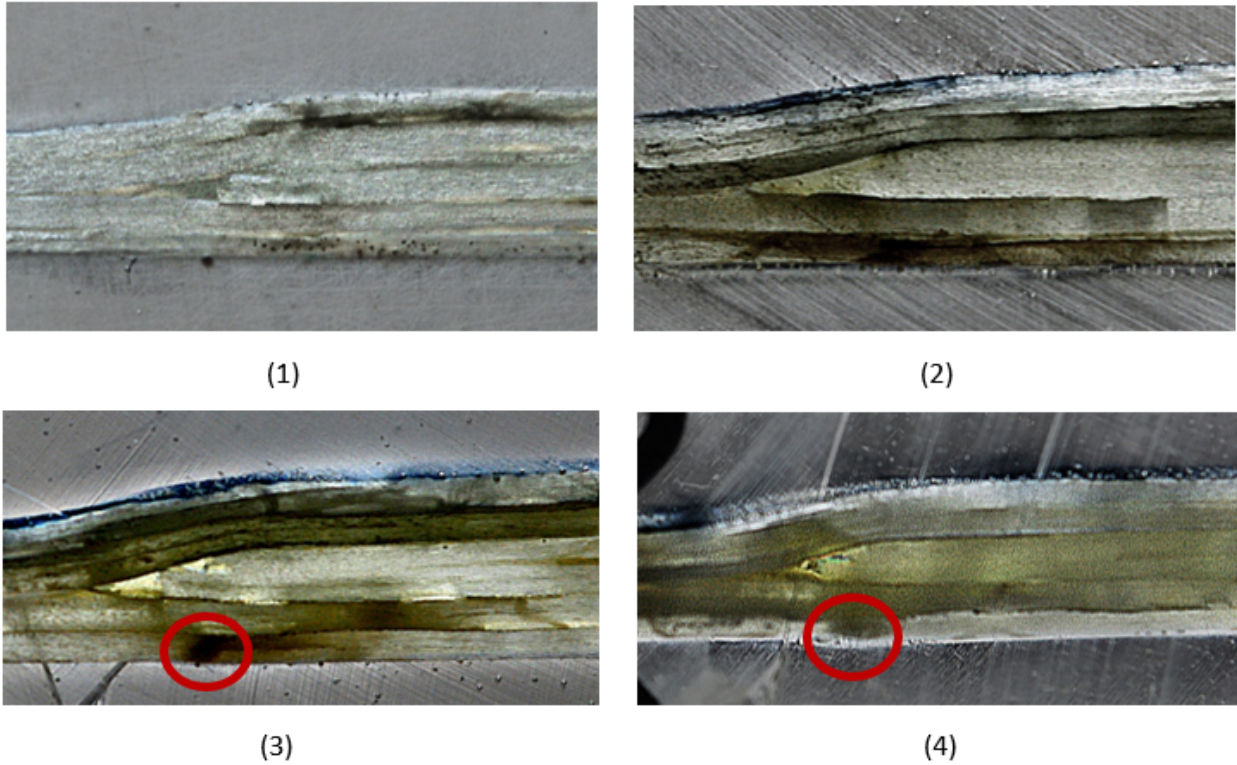


Figure 11: Ply drop failure development.

Cuts shown in Figure 11 are 1 millimetre far from each other. And the following crack development is identified:

1. Very beginning of the crack where damage is not still visible.
2. Delamination occurs both over and below the ply drop.
3. Delamination is clearly visible and kink band failure seems to appear at the bottom layer due to shear microbuckling [12].
4. Kink band of the bottom layer leads to fibre failure.

4. Modelling

The purpose of building a reliable finite element model is to be able to analyse in dept stress fields developed in the component and predict the first failure incident. Abaqus [13] is the software used throughout this analysis.

4.1. Model development

Geometry of the tube is drawn making use of symmetry conditions. As it has two symmetry planes ($x - z$ plane and $x - y$ plane), just one quarter of the cylinder is considered. The steel round plate that supports the tube in the actual experiment is modelled as a square solid of very high stiffness attached to the tube. This way, it will not exhibit any deformation and all strain energy will be directed to the composite specimen. Both elements are bonded together to ease the model. At the upper surface of the plate model, semicircular areas are created to introduce the load in order to resemble the experimental test.

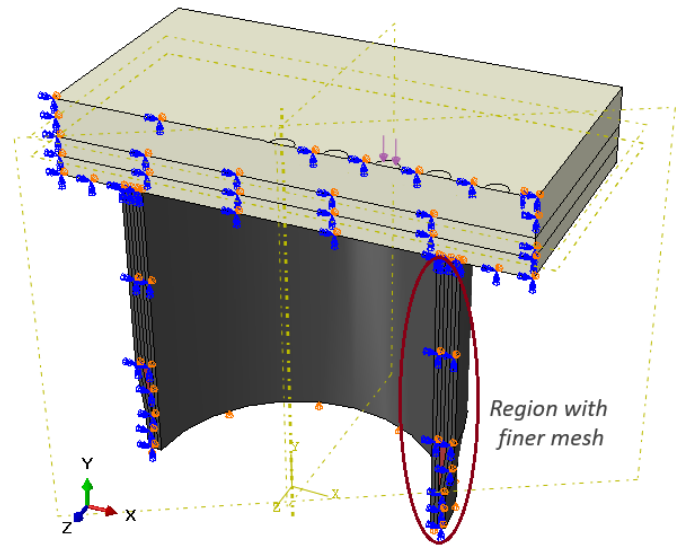


Figure 13: Image of the finite element model when symmetry conditions are applied. Boundary conditions and load are shown.

Movement of the lower surface is prohibited in y axis as the setup is symmetric with respect to the $x - z$ plane. Also, symmetry is applied in the $x - y$ plane setting displacement in z and rotations along x and y axis equal to zero. Load is applied as a pressure onto any of the aforementioned circular surfaces. For instance, in Figure 13, the load is applied at the third surface, equivalent to an eccentricity of $2/3$ of the radius length (second experimental setup). The whole model is meshed by the

use of an 8-node linear solid element with reduced integration and hourglass control (C3D8R in Abaqus). Reduce integration is chosen to reduce the simulation time and increase computational efficiency but it may lead to shear locking hence hourglass control is employed. A finer mesh is used at the edge closer to where the force is applied (region marked in Figure 13) as it will develop higher stresses and it is the location of more interest. Several partitions are made along the model to make the meshes compatible, and mesh technique varies between structural and sweep mesh depending on the part.

4.2. Model validation

The elastic response to the model is validated by comparing strains obtained with strain gauge measurements from the experimental test with model prediction. For a loading case of 100 kN, a path is set in the model running from 0° strain gauge location to 180° (Figure 9) and strains are displayed. Values of the strain gauges are plotted as well for comparison. It is seen in Figure 14 that both measurements remain the same order and are close to each other. Nevertheless, it is appreciated that the model is slightly less stiff than the real composite which can be caused by the reduced integration. Model is considered as valid and reliable.

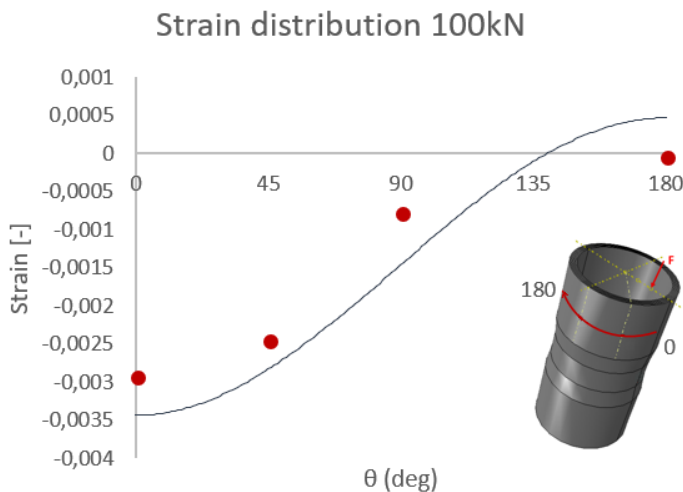


Figure 14: Strain gauge measurement (red dots) compared to model strains for 100 kN of applied force along a circumferential path.

It stands out that the finite element model shows positive strains at the back part of the cylinder (between 135° and 180°). This is caused by the bonding restriction between the two solids in the model, which implies that they must be in contact no matter the load condition, leading to traction stresses (positive strains) at the back part of the cylinder.

4.3. Stress fields away from ply drop location

Stresses are evaluated far from the ply drop where its presence does not have an influence yet. The reason for this study is to compare the stress state of the tube under compression and check if it is comparable to a flat type specimen. The distance away from the ply drop has been agreed to be two times

the thickness of the thin part component. Two paths through the thickness (named *Length x₂* in Figure 15) are drawn at this locations and stresses evaluated throughout it for 100 kN of applied force at 2/3 of the radius length measured from the centre.

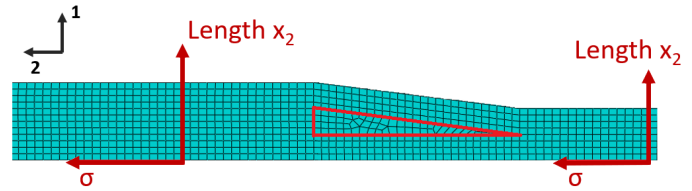


Figure 15: Horizontal sketch of the two paths drawn to represent different stresses. Material coordinate system is shown in the upper left corner.

Shear stresses σ_{13} and σ_{23} are too small compared to the rest of the stress components so they will not be taken into account as their influence is minimal.

Figure 16 represents the stress state of the composite tube when is loaded under both compression and bending.

- Transverse stresses become ten times higher at the thick part of the composite tube compared to the thin part. In any case, at both edges they are zero and increase as the centre is approached. Transverse stresses are endured by the thick part of the composite.
- Longitudinal stresses are similar at the inner part of the tube and they separate as the outer part is approached. Thick part shows a slight decrease of stresses but in general remain quite constant. However, longitudinal stresses increase at the thin part of the tube. This implies that the region that withstands more longitudinal stresses is the outer surface of the thin part.
- Shear stresses become four times higher at the thick part of the tube compared to the thin. As seen from the graph, shear σ_{12} is very small at the two outer layers of the thick part, but increases rapidly at the inner layers. The peak along both paths is located at the length 4 which correspond to the interface between layers two and three, and could ease delamination at this location.

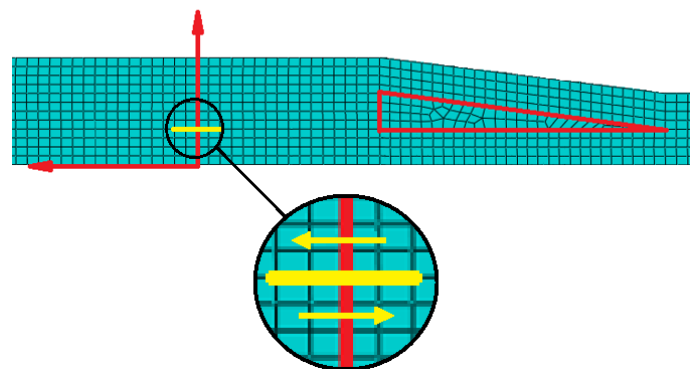


Figure 17: Shear stresses σ_{12} show a peak at the yellow location that eventually could lead to delamination initiation.

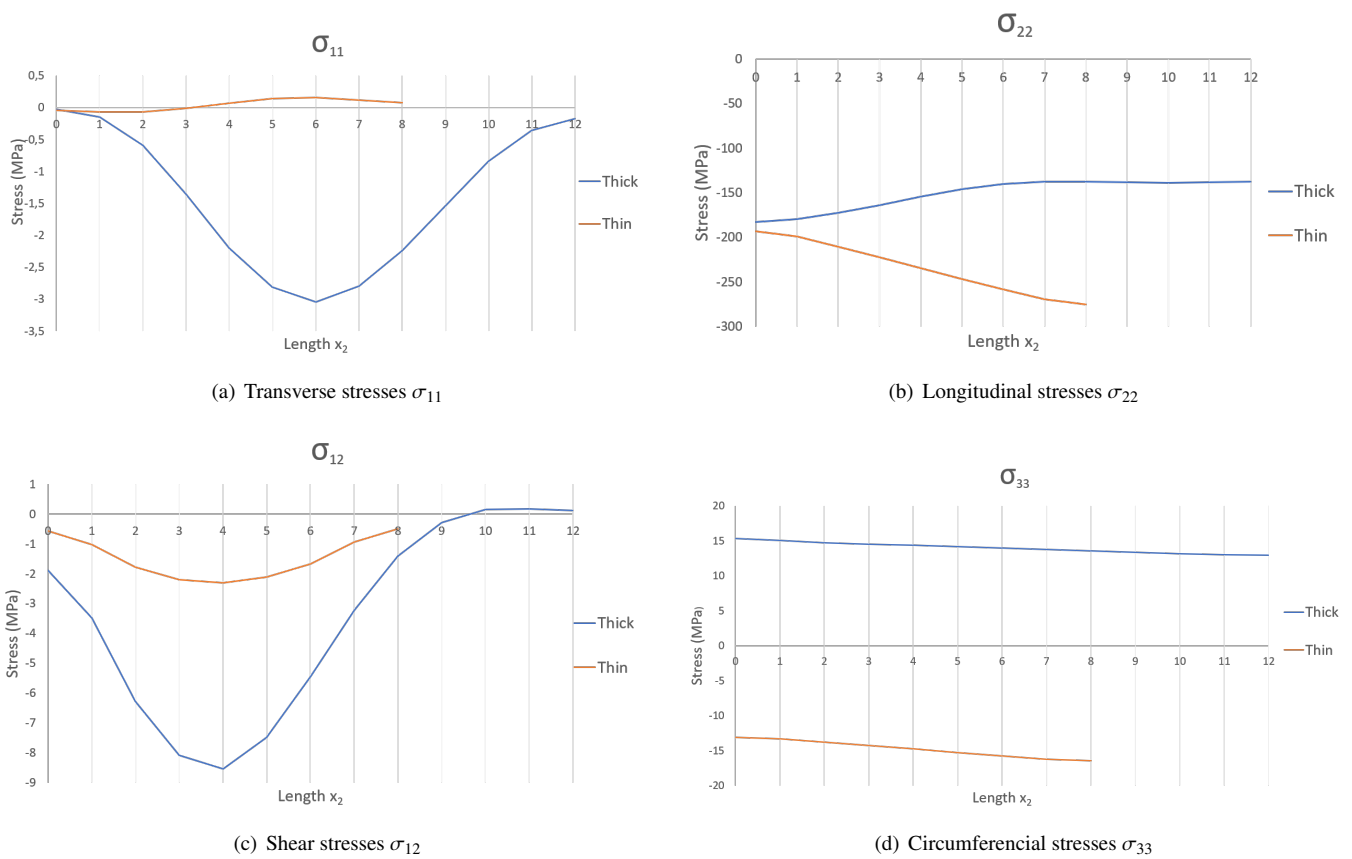


Figure 16: Stress components along both thin and thick paths in cartesian coordinate system. Origin is at the inner part and moves outwards.

d) Circumferential stresses σ_{33} are of the same magnitude at both sides of the tube but opposite sign. This is caused as the thin part is bent inwards, producing compressive stresses (negative sign), while the thick part is pulled outwards, leading to tensile stresses (positive sign) at that part. This behaviour is sketched in the following figure:

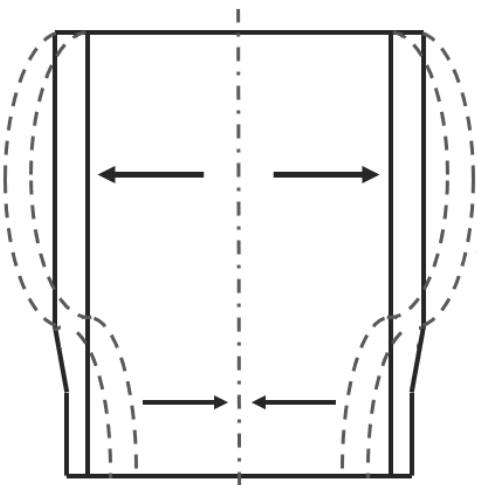


Figure 18: Cross section sketch of the deformed upper half composite tube. Stresses at the upper part (thick) are positive, meaning traction. Stresses at the lower part (thin) are negative, which corresponds to compression.

4.4. First failure incident prediction

To determine the first failure incident, stresses around the ply drop are evaluated since it is the critical point of the structure. First, it is important to empathise that σ_{11} becomes singular at the corner of the ply drop due to the sudden change of material that implies material discontinuity. Hence, a convergence study is performed setting a path that approaches that critical point. Two different meshes are tested: coarse with a element size of 1 mm and fine whose element size is 0.5 mm, when 100 kN is applied at 2/3 radius length measured from the centre:

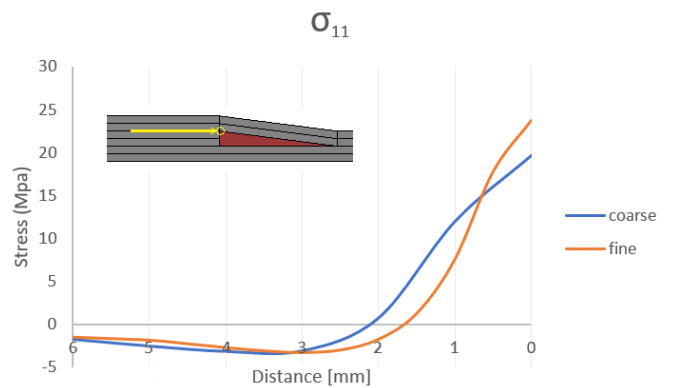


Figure 19: Stresses σ_{11} when approaching the ply drop corner.

Transverse stresses become positive at 2 mm from the ply drop, which ease the crack opening but keep increasing to unreal levels at the last element due to singularity. St. Venant principle states that the effect of a singularity is purely local meaning that sufficiently far away from a singularity the solution is appropriate ([14],[15] and [16] explained in Appendix E). One thickness away of the singularity stresses converge, then it is decided to disregard the last value and conduct the following studies with the value obtained at the previous element, equivalent to stresses one ply thickness away.

The approach to predict the first failure incident is by calculating the force needed to reach the ultimate strength. As seen in Section 3, first failure will occur at the upper corner of the ply drop (region 1) and afterwards it extends to the two internal plies of the composite (below the ply drop, region 2), so both regions are studied. For the first case, stresses that could eventually provoke delamination are both *Transverse stresses* (σ_{11}) or *Shear stresses* (σ_{12}), as these are of biggest magnitude and would create the first failure incident. Once failure has occurred at region 1, next failure incident happens at region 2, so it is checked that when the first failure incident occurs, region 2 is still safe. Calculations are also verified by obtaining the Failure Index (FI) by the use of either of these expressions depending of the case:

$$FI = \left(\frac{\sigma_{11}}{S_{11}}\right)^2 + \left(\frac{\sigma_{12}}{S_{12}}\right)^2 \geq 1 \quad (\text{at region 1})$$

$$FI = \left(\frac{\sigma_{22}}{S_{22}}\right)^2 + \left(\frac{\sigma_{12}}{S_{12}}\right)^2 \geq 1 \quad (\text{at region 2})$$

Table 3 contains the first failure incident calculation for three different loading cases depending on the eccentricity of the load.

At all cases, *Transverse stresses* (σ_{11}) are the ones that initiate delamination and thus failure at the upper corner of the ply drop. Failure indices support that the inner plies under the ply drop are still undamaged. Experimental tests have shown that when the load is applied aligned to the central axis (case 1), the specimen could endure up to 188 kN of force applied, and the model predicts failure at 211 kN. This implies an error of

12%. When the load is applied at 2/3 the radius length measured from the centre (case 3), the specimen tested showed the first delamination (Figure 8) when 110 kN were applied, and model predicts that delamination initiates at 94.7 kN. Error for this case is 13.9%.

5. Conclusion

Within this work, a unidirectional composite tube has been tested under a combined compression and bending load. Experimental data showed a gradual failure for tubes loaded with an eccentric force ($a = 2R/3$). The final failure occurred at 140 kN compared to a failure load of 188 kN for a concentric loaded tube ($a = 0$). For the eccentric loaded tube, a subsequent analysis by the use of a high-speed camera identified that the first failure mechanism was delamination at the ply drop location initiating at 110 kN. Samples from the damaged area were cut and prepared for microscopic investigations. Here it was confirmed that a possible first failure incident was delamination in the vicinity of the ply drop. Secondly it is proposed that the combination of shear and compression stresses lead to micro-buckling of the inner layers and resolved in kink band formation and finally fibre failure.

Through finite element analysis, stresses were analysed for the aforementioned loading state. Transverse stresses near the ply drop reached first the material strength, meaning that they were responsible for delamination as they tend to "separate" the plies. Delamination load could be predicted with an error of 13.9%. Stresses evaluated through the thickness of the tube away from the ply drop showed the stress state of the tubular composite which is slightly more complex compared to a "flat type specimen". Therefore, it is not expected that results can be directly compared between the two test methods (flat and tube specimens). However the tube may be used as a well-controlled benchmark case for compression models of composites with embedded ply drop.

Loading case	Region	Critical stress	Material Strength	Model for 1 kN	Force to failure	FI
	1	S_{11}	36 MPa	0.17 MPa	211 kN	1.065
		S_{12}	55 MPa	0.07 MPa	785 kN	
	2	S_{22}	579 MPa	-1.35 MPa	428 kN	0.4907
		S_{12}	55 MPa	0.13 MPa	423 kN	
	1	S_{11}	36 MPa	0.28 MPa	129 kN	1.086
		S_{12}	55 MPa	0.12 MPa	458 kN	
	2	S_{22}	579 MPa	-2.26 MPa	256 kN	0.352
		S_{12}	55 MPa	-0.21 MPa	261 kN	
	1	S_{11}	36 MPa	0.38 MPa	94.7 kN	1.0806
		S_{12}	55 MPa	0.166 MPa	331.3 kN	
	2	S_{22}	579 MPa	-3.17 MPa	182.65 kN	0.5356
		S_{12}	55 MPa	-0.3 MPa	183.3 kN	

Table 3: Failure load and Failure Index (FI) for the different loading cases.

References

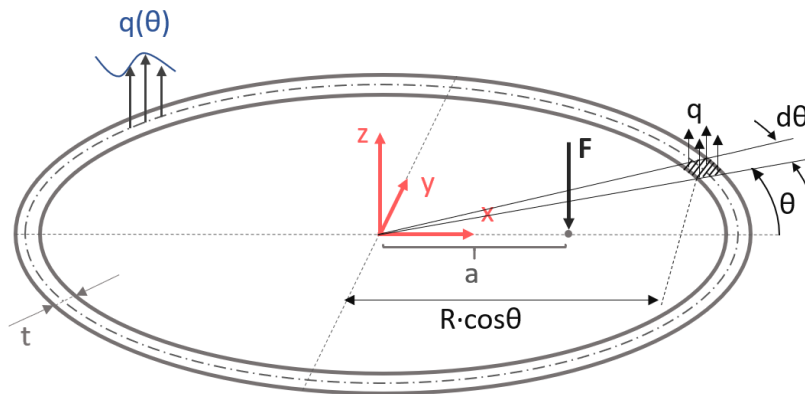
- [1] P. M. Jelf, N. A. Fleck, The failure of composite tubes due to combined compression and torsion. *Journal of Materials Science* (1993) 3080–3084.
- [2] A. M. Harte, N. A. Fleck, Deformation and failure mechanisms of braided composite tubes in compression and torsion. *Acta Materialia*, Volume 48 (2000) 1259–1271.
- [3] C. J. McGregor, R. Vaziri, A. Poursartip, X. Xiao, Simulation of progressive damage development in braided composite tubes under axial compression. *Composites Part A: Applied Science and Manufacturing* (2007) 2247–2259.
- [4] E. F. Abdewi, Experimental Testing of Composite Tubes with Different Corrugation Profile Subjected to Lateral Compression Load. *International Journal of Mechanical and Mechatronics Engineering*, Vol. 7. (2013) 183–186.
- [5] E. F. Abdewi, S. Sulaiman, A. M. S. Hamouda, E. Mahdi, Quasi-static axial and lateral crushing of radial corrugated composite tubes. *Thin-Walled Structures*, Volume 46 (2008) 320–332.
- [6] I. M. Daniel, H.-M. Hsiao, S.-C. Wood, Failure mechanisms in thick composites under compressive loading. *Composites Part B*, 27B. Elsevier. (1996) 543–552.
- [7] J. Wang, K. D. Potter, M. R. Wisnom, K. Hazra, Failure mechanisms under compression loading in composites with designed out-of-plane fibre waviness. *Plastics, Rubber and Composites*. (2013) 231–238.
- [8] C. A. Steeves, N. A. Fleck, Compressive strength of composite laminates with terminated internal plies. *Composites Part A: Applied Science and Manufacturing*, Volume 36 (2005) 798–805.
- [9] H.-W. Song, X.-W. Du, Off-axis crushing of GFRP tubes. *Composites Science and Technology*, Vol. 62. (2002) 2065–2073.
- [10] S. A. R. Hosseiny, J. Jakobsen, Fatigue damage simulation of Tension-Tension Loaded glass/polyester fiber composites with thickness tapering effects. *Journal of composite materials*.
- [11] K.-T. Hsiao, D. Heider, 10 – Vacuum assisted resin transfer molding (VARTM) in polymer matrix composites. *Manufacturing Techniques for Polymer Matrix Composites (PMCs)*. (2012) 310–347.
- [12] L. C. T. Overgaard, *Mechanics of Composite Materials and Structures - Failure Criteria Part 1*, 1st Edition, Aalborg University, 2014.
- [13] Dassault Systèmes, *Abaqus manual 6.10*, (2012).
- [14] E. T. Camponeschi, *Composite Materials: Testing and Design* (eleventh volume), ASTM International, 1993.
- [15] J. R. Barber, *Solid Mechanics and its applications*, Kluwer Academic Publishers, 2003.
- [16] J. M. Gere, S. P. Timoshenko, *Mechanics of Materials*, PWS-Kent Publishing Company, 1984.

APPENDIX



Stress distribution along circular annulus surface

When a force F is applied at any point on a circular annulus some reaction $q(\theta)$ is expected in the round surface following an unknown q distribution that depends on the angle θ .



In order to obtain the stress distribution function, force equilibrium in z axis is applied as well as momentum equilibrium with respect to y axis:

- Eq. force in z :
$$\sum F = -F + \int_0^{2\pi} q(\theta) \cdot t \cdot R \cdot d\theta = 0$$
- Eq. momentum in y axis:
$$\sum M = F \cdot a - \int_0^{2\pi} (q(\theta) \cdot t \cdot R \cdot d\theta) (R \cdot \cos\theta) d\theta = 0$$

Stress distribution will follow a function on the form: $q(\theta) = q_1 + q_2 \cdot \cos\theta$

Isolating F in both above equations:

- Force equilibrium:
$$F = t \cdot R \int_0^{2\pi} q(\theta) \cdot d\theta$$
- Momentum equilibrium:
$$F = \frac{t \cdot R^2}{a} \int_0^{2\pi} q(\theta) \cdot \cos\theta \cdot d\theta$$

Introducing the solution to both equations:

$$F = 2 \cdot t \cdot R \cdot q_1 \cdot \pi \longrightarrow q_1 = \frac{F}{2 \cdot \pi \cdot R \cdot t}$$

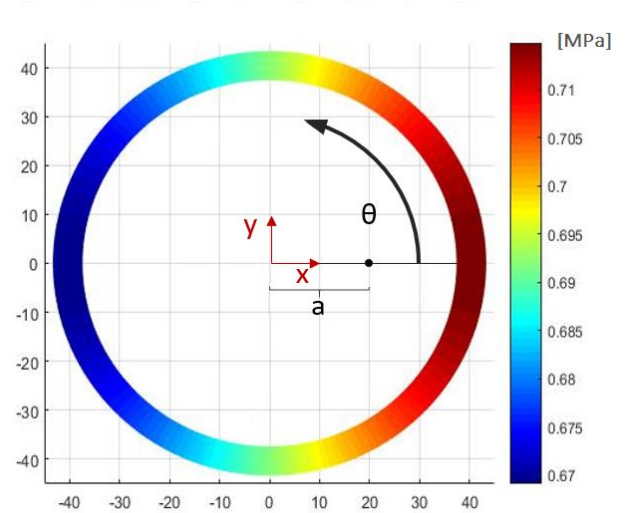
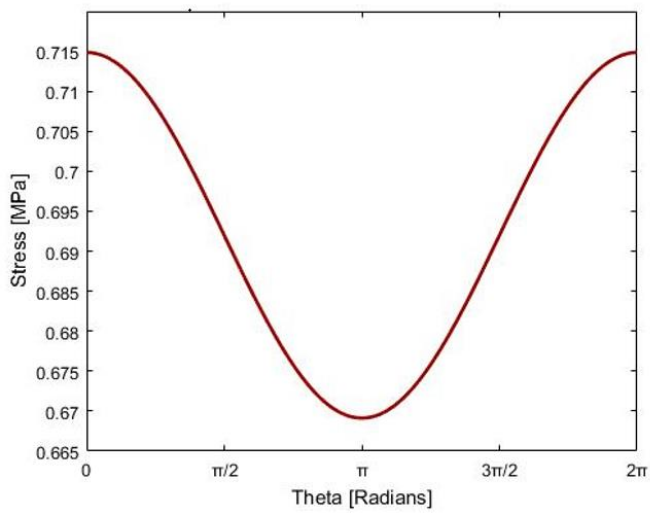
$$F = \frac{1}{a} \cdot t \cdot R^2 \cdot q_2 \cdot \pi \longrightarrow q_2 = \frac{F \cdot a}{\pi \cdot R^2 \cdot t}$$

Introducing q_1 and q_2 to the solution form, the stress distribution function around the circular surface is obtained:

$$q(\theta) = \frac{F}{2 \cdot \pi \cdot R \cdot t} + \frac{F \cdot a \cdot \cos\theta}{\pi \cdot R^2 \cdot t}$$

Considering the specimen dimensions, an eccentricity of $2R/3$ and a force of 1 kN, the stress distribution takes the form:

- $F = 1000$ N
- $a = 2/3$
- $R = 40.35$ mm (central radius)
- $t = 5.7$ mm (measured from the specimen)



B

Experimental setup pictures

This appendix includes the experimental test setup pictures. All the tests were performed in the same way: specimen was held in between two round steel plates and placed in the Schenk machine. Rubber bands were used to maintain the plates and the specimen as a whole. Two sources of light located at each side of the specimen would improve the view of its surface. Finally, a safety glass was placed in between the specimen and the viewers to avoid possible shavings.



Figure B.1. Experimental test setup.

In order to introduce the compression force to one specific location, two steel balls were used at both specimen endings. Figure B.2 show the eccentric loading case. A wooden stop was placed around the ball to prevent the steel plates to lean too much and fall.



Figure B.2. Steel ball that concentrate the load to one point.

Figure B.3 show the specimen with the strain gauges mounted in. The weld of the wires to the gauges is likely to break with a small movement of the wires, so tape was used to secure them.

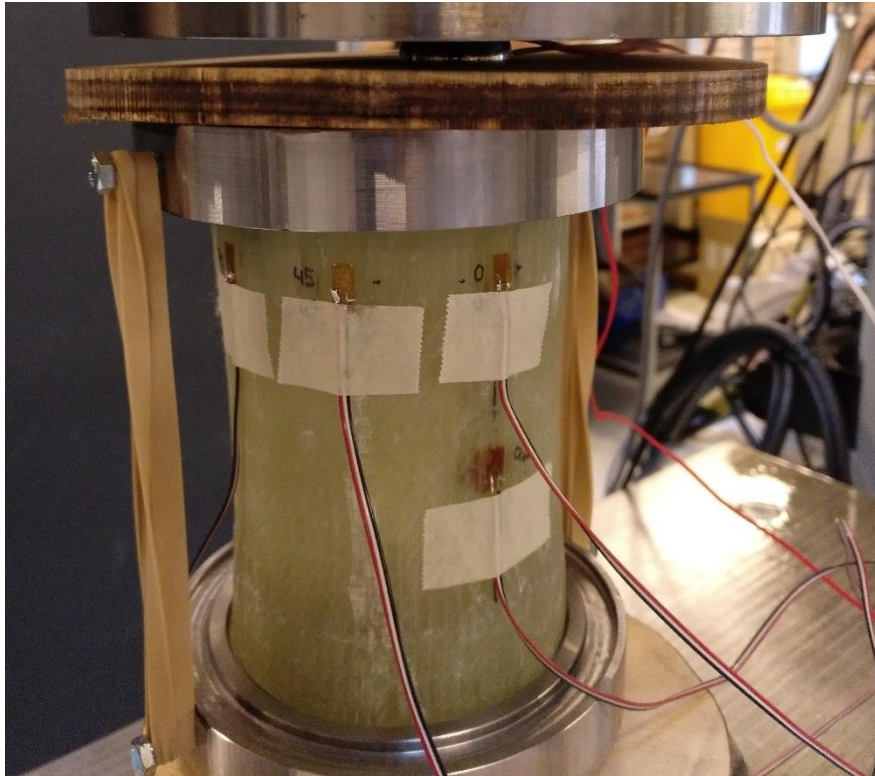
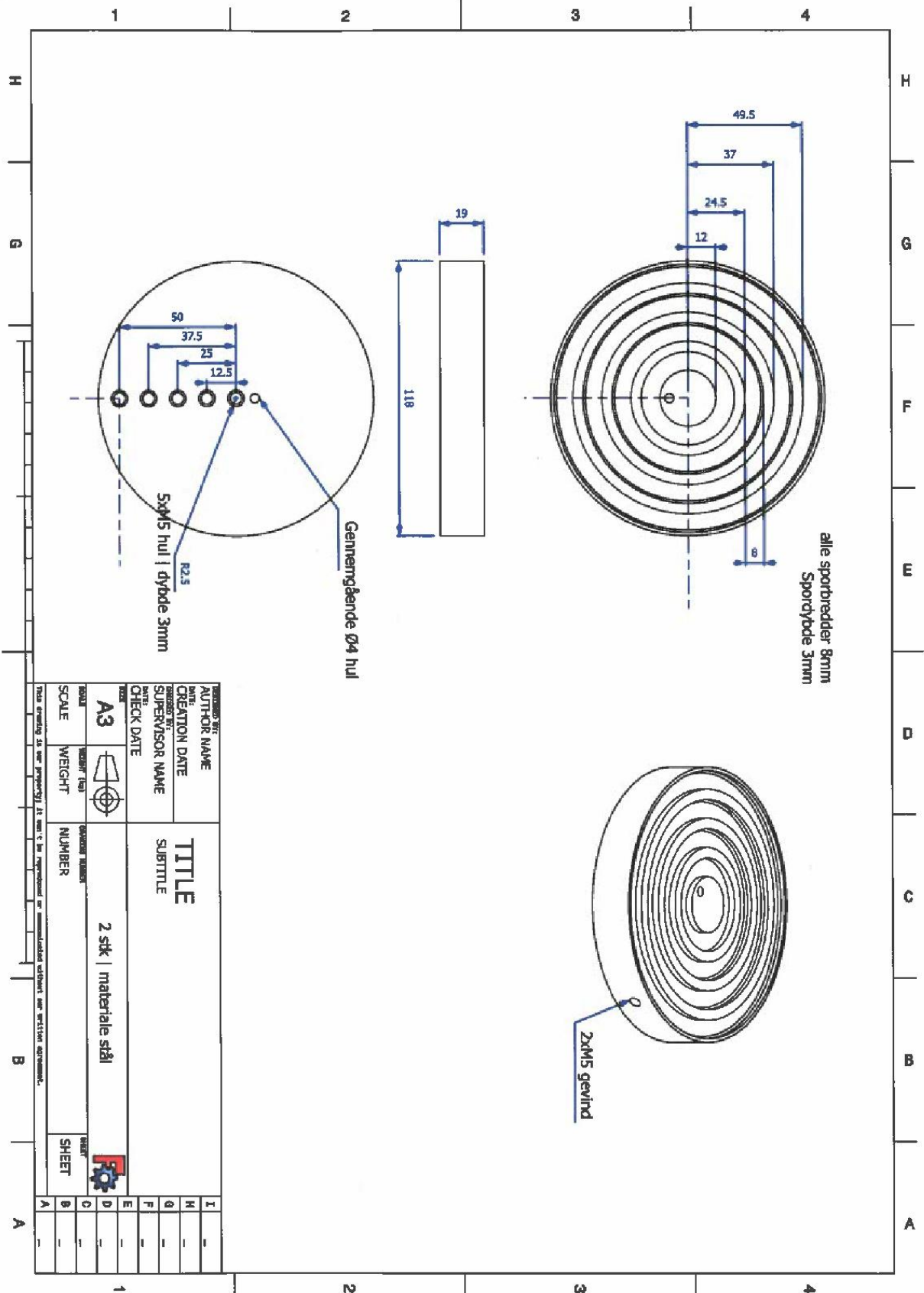


Figure B.3. Strain gauges mounted on the specimen.



Steel plate technical drawing



D

Broken specimen pictures

This appendix contains the pictures of the specimens after failure. In the first test performed, the compression load was applied aligned with the center of the tube. Stress distribution was uniform along the tubular specimen, which led to a continuous failure around its diameter.



Figure D.1. Specimen under centered compression after failure. Damage is visible around the whole cylinder.

When the load was applied eccentrically, damage was only caused to the half of the cylinder under higher pressure. In this case, cuts were performed at different angles (see Figure 12 of the paper) that are also shown here.



Figure D.2. The crack front occupies the half of the cylinder under higher pressure.

0° Cut



Here the highest damage was expected as this cut was done at the point with higher stress. Delamination is visible at the upper layers of the ply drop as well as fibre failure at the bottom part.

30° Cut



Damage looks similar as at the previous cut. Delamination at the upper layers of the ply drop and fibre failure at the bottom.

45° Cut



No difference with the previous cuts. Still delamination and fibre failure.

60° Cut



Delamination at the upper layers seem to be less abrupt. Fibres at the bottom part failed forming a kink band due to shear micro buckling.

90° Cut



Cut performed at the very beginning of the crack front but damage is not visible yet.

105° Cut



No damage visible. Ply drop remained intact at the other half of the cylinder.



Singularities in Finite Element Analysis

Finite Element Analysis (FEA) allows to obtain a solution to a physical problem by discretizing a continuum domain into small finite elements, called mesh. The accuracy of the solution depends on the number and size of the elements used to represent the physical domain. The smaller the elements are, the better the result is. Then progressively refining the mesh, solution will converge to the exact solution. However, it could happen that the solution does not converge with mesh refinement. This happens at stress singularities. A stress singularity is a point on the mesh where stresses keep increasing with mesh refinement. Theoretically, stress at a singularity is infinite.

Typical stress singularities are: point loads, sharp corners, contact points between bodies, sudden change of material properties... These are common features in FEA, nevertheless it does not mean that model results are incorrect. Some distance away from the singularity, stress results are correct, which is a consequence of the St. Venant's Principle.

St. Venant's Principle states that the effect of a stress singularity is purely local, thus stresses decay rapidly with distance. The decay rate is likely to be related to the width of the loaded region.

“If we move away by an amount equal to the width of the bar from a point of loading, from a reaction, or from any other stress concentration, the effect of the stress concentration will become insignificant and the stresses can be calculated by the usual mechanics of materials formulas. [...] Since the stress concentration effects are highly localized, any related displacement formulas give accurate results even when stress concentrations are present”

[Gere, M. J. and Timoshenko, S. P. (1984) *Mechanics of Materials.*] (p 120)

Sources:

- Camponeschi, E. T. (1993) *Composite Materials: Testing and Design (eleventh volume)*. ASTM International. (p 32)
- Barber, J. R. (2003) *Solid Mechanics and its applications*. Kluwer Academic Publishers. (p 71)
- Gere, J. M. and Timoshenko, S. P. (1984) *Mechanics of Materials*. PWS-Kent Publishing Company. (p 120)
- Murakami, Y. (2017) *Theory of elasticity and stress concentration*. John Wiley & Sons, Ltd. (p 48)